Intrinsic Transparent Conductors without Doping

Xiuwen Zhang, Lijun Zhang, John D. Perkins, and Alex Zunger

Phys. Rev. Lett. **115**, 176602 — Published 23 October 2015

DOI: 10.1103/PhysRevLett.115.176602

Intrinsic transparent conductors without doping

Xiuwen Zhang[1], Lijun Zhang[1, †], John D. Perkins[2], and Alex Zunger[1, *]

[1]University of Colorado, Boulder, CO 80309, USA

[2]National Renewable Energy Laboratory, Golden, CO 80401, USA

*Corresponding author Email: alex.zunger@colorado.edu

Transparent conductors (TC's) combine the usually contraindicated properties of electrical conductivity with optical transparency and are generally made by starting with a transparent insulator and making it conductive via heavy doping, an approach that generally faces severe 'doping bottlenecks'. We propose a different idea for TC design—starting with a metallic conductor and designing transparency by control of intrinsic interband transitions and intraband plasmonic frequency. We identify the specific design principles for three such prototypical intrinsic TC classes and then search computationally for materials that satisfy them. Remarkably, one of the intrinsic TC, $Ag_3Al_{22}O_{34}$, is predicted also to be a prototype 3D compounds that manifest natural 2D electron gas (2DEG) regions with very high electron density and conductivity.

†Present address: College of materials science and Engineering, Jilin University, Changchun 130012, China

The functionality of transparency plus conductivity [1, 2] lies at the center of many technological applications such as solar cell, touch-screen sensors, light emitting diode, electronic papers, infrared or ultraviolet photo detector, smart windows and flat panel display [1-9], yet materials with such seemingly contraindicated properties are difficult to come by. The traditional strategy for searching TC's has followed the path illustrated by the arrow in Fig. 1(a): start from a transparent insulator and find ways to make it conductive by doping it extensively without affecting its optical transparency [1-9]. Successful examples are very few and include electron doped ZnO, Sn-doped In_2O_3 and La-doped $SrGeO_3$ for electron-conducting (*n*-type) TC's [3, 4, 7, 8], as well as hole doped $CuAlO_2$ and K-doped $SrCu_2O_2$ for hole-conducting (*p*-type) TC's [5, 9]. The limiting factors are rooted in defect physics [10-12] and include difficult to fulfill requirements such as finding wide-gap insulators that can be amply doped without promoting carrier compensation or structural deformations.

In this Letter, we revisit the basic physics design principles needed for transparent conductivity and find that a different, previously overlooked route, illustrated by the arrow in Fig. 1(b), may be possible—start from an opaque conductor that already has plenty of free carriers, then design optical transparency to realize an intrinsic (i.e., without intentional chemical doping) TC. However, not all bulk conductors will do; one needs to search for bulk metals that (a) have a sufficiently broad energy window in their electronic structure either below the Fermi energy E_F (for *n*-type TC) or above E_F (for *p*-type TC), so the interband transitions across the 'energy window' will not obscure optical transparency, and (b) do not have a high plasma frequency (ω_p) [13] (such as ~15 eV/ħ for Al [13]) so the free carrier reflection will not limit transparency. If one can find metals that satisfy such conditions this would results in the interesting case of metallic conductivity in a transparent and pristine (undoped) crystal. This approach is applicable to *bulk compounds* thus is different from the approach of using ultra thin films of metallic materials that are transparent only when they are kept ultra thin [14-17].

The two conditions noted above can appear unusual and indeed materials satisfying them have, to our knowledge, not been deliberately searched before. Here, we illustrate the concept of intrinsic TC by discussing first simple, hypothetical structures of RbTe in

the NaCl structure and highly compressed crystalline silicon in the diamond structure, followed by realistic but more complex metallic ceramics reported as having been previously synthesized (but not characterized for conductivity or transparency) in the ICSD compilation of inorganic structures [18] as well as in specific literature on $Ag_3Al_{22}O_{34}$ in the hexagonal P63/mmc structure [19] and $Ba_3Nb_5O_{15}$ in the tetragonal P4/mbm structure [20]. In addition, using first principles thermodynamics based on DFT, we have computed their stability with respect to many possible competing phases, as described in the Supplementary Section I. Whereas these compounds, screened theoretically according to our design principles from hundreds of possibilities, are by no means optimized for maximal functionality, they clearly demonstrate the viability of the concept of intrinsic transparent conductors without doping. Remarkably, the free electrons predicted to exist in $Ag_3Al_{22}O_{34}$ are found to be spatially organized as *two dimensional electron gas (2DEG), periodically embedded in the 3D compound.*

To study the prototype behaviors of intrinsic transparent conductors, we evaluate their electronic structures, dielectric function, plasma frequency and optical properties by the density functional theory (DFT) [21, 22] as well as hybrid functional (HSE06) [23] (see Supplementary Sections II and III for details).

Type-1 intrinsic TC are metals with an isolated intermediate-band: The first type (ITC-1) illustrated in Fig. 2 is based on metallic, intermediate-band (IB) materials where the IB is energetically isolated from the bands below and above it and the Fermi energy is located within that band. The particular example shown is based on RbTe in the zincblende crystal structure (Fig. 2(a)) with electronic structure shown in Fig. 2(b).

The *general* required design principles for this prototype (ITC-1) include: (i) the bands above the IB and the bands below IB need to be separated by broad energy windows from the IB (see e.g. Fig. 2(b)) so as to prevent interband transitions by visible light photons. (ii) The energy spacing between different subbands within the IB needs to be smaller than visible light photon energy (Fig. 2(b)) so as to prevent inter-subband transitions with visible-light photon energies. The way the narrowness of the IB helps to defeat inter-subband absorption can also be used in conventional, chemically doped p-type TC's—such narrow bands could lead to high transparency, free of inter-valence-bands

transitions. (iii) The carrier density partially filling the IB needs to be in the region that gives a plasma frequency lower than the frequency of visible light but high enough for good conductivity [24] $\sigma = \frac{(\omega_p)^2}{4\pi\gamma}$ where γ is the damping coefficient [24] (we use $\gamma = 0.2$ eV/ħ analogous to traditional TC's [7]). The need to satisfy such multiple electronic structure functionalities is key to identification of such rare compounds. Fortunately, this is possible, as shown below.

Following these design principles, we focused our attention on the I-VI compounds (I = Rb and VI = Se, Te) in the zincblende (ZB) structure, the reasons being that such sub-octet I-VI compounds have a partially filled chalcogen *p*-band that is energetically isolated from the alkali ion *s* bands above it and from the chalcogen ion *s* bands below it, thus forming a separate intermediate band (see e.g. Fig. 2(b)). Zincblende RbTe is found to satisfy the conditions for ITC-1 rather well: the bulk optical absorption coefficient (Fig. 2(c)) including plasmonic effect based on Drude model [24] shows nearly zero optical absorption for most visible light. The plasma frequency [24] $\omega_p \sim \sqrt{n_h/m^*}$ (0.56 eV/ħ) is low enough for transparency due to the large effective mass m^* of IB, but high enough for good conductivity (0.21×10^3 S/cm) due to the high hole density ($n_h = Z/a^3 = 6.71\times10^{21}$ cm^{-3} where $Z = 4$ is the number of holes in the unit cell and a = 8.42 Å is the calculated lattice constant). Indeed the simulated optical reflection and transmission spectra for a free standing 1 μm thick slab with optically smooth surfaces (Fig. 2(d)) shows that the sample has very high transmittance (T) and low reflectance (R) for most visible light. Analogous results for ZB RbSe are shown in Supplementary Fig. S4. However, we find that the ZB structure of RbTe (RbSe) is higher in energy than their Na_2O_2-type ground state structures [18] by 0.655 (0.701) eV/atom. We caution that in general the predicted intrinsic TC properties hold for the crystal structure and composition used in the prediction—other structures or compositions need not have the same ITC properties.

Type-2 intrinsic TC is an indirect gap semi-metal with large direct band gaps: The ITC-2 type is based on semimetals having a large *vertical* band gap (assuring optical transparency), yet a zero *indirect band gap*, assuring semi-metallic behavior. The

particular example shown is based on compressed silicon in the diamond-type (Fd-3m) structure (Fig. 3(a)) with DFT electronic structure calculations shown in Fig. 3(b).

The *general* required design principles for this prototype (ITC-2) include: (i) large direct gap above the photon energy of most visible light between the $(N_e)^{th}$ and $(N_e+1)^{th}$ bands (N_e is the number of electrons in the primitive cell) so the optical transition between them does not affect the transparency for visible light, and a zero indirect gap. This requires the $(N_e)^{th}$ and $(N_e+1)^{th}$ bands to be highly dispersive and nearly parallel in a portion of the Brillouin zone (e.g. along the Γ-X direction in Fig. 3(b)). (ii) The carrier densities (equal amount of electrons and holes) need to be low enough to achieve a small plasma frequency and a weak optical transition of the electrons (holes) from the $(N_e+1)^{th}$ ($(N_e)^{th}$) band to higher (lower) bands.

Diamond-type (Fd-3m) Si at high pressure (50 GPa) is chosen to illustrate the design principles although this structure is not the stable phase for highly compressed silicon (for pressure higher than ~11.2 GPa, Si transforms [25] into the β-Sn $I4_1/amd$ structure that is an opaque metal with calculated plasma frequency > 9 eV at pressures 0~50 GPa). Within this caveat, compressed Si is found to satisfy the conditions for ITC-2 rather well: the low carrier concentration ($n = 0.08\times10^{21}$ cm^{-3}) leads to low plasma frequency (0.58 eV/ħ). Indeed the evaluated absorption coefficient (Fig. 3(c)) is nearly zero for most visible light and very small for infrared light. The transmittance (Fig. 3(d)) is mainly limited by the reflectivity that shows strong oscillatory pattern due to the coherent internal reflections. In actual technological applications, this can be largely mitigated through the use of antireflection coatings or optically rough surfaces.

Type-3 intrinsic TC is a near-octet metal: The third type of intrinsic TC is based on metallic compounds that have a near-octet electronic structure. The particular example shown (Fig. 4(a)) is based on $Ag_3Al_{22}O_{34}$ in the hexagonal $P6_3/mmc$ structure [18] (inset of Fig. 4(b)). Considering the standard formal charges of the constituents Al = 3+, Ag = 1+ and O = 2-, the compound $Ag_3Al_{22}O_{34}$ would have $1\times3 + 3\times22 - 2\times34 = +1$ nonzero residual valence per formula unit (the *net* physical charge is, however, zero as the nuclear charges compensate the electronic charges). Such near-octet compounds can be made, among other methods, by starting with wide gap octet insulator such as $Ca_{12}Al_{14}O_{33}$ [6]

and reducing it to $Ca_{12}Al_{14}O_{32}$ [26], which is a metal. This example, tried previously [26], however, is not really transparent (see Supplementary Fig. S5).

The *general* required design principles for this prototype (ITC-3) include: (i) The $(N_e-\delta)^{th}$ and $(N_e-\delta+1)^{th}$ bands (N_e is the number of electrons and δ is the residual valence per primitive cell) need to be separated by a large energy window (see e.g. Fig. 4(a)), so the interband optical transition across the energy window does not affect the transparency for visible light. (ii) The carrier density (n) and dispersion of the partially filled bands (see Fig. 4(a)) need to be sufficiently low for low plasma frequency [24] $\omega_p \sim \sqrt{n/m^*}$. (iii) The optical transition of the electrons (holes) from the partially filled bands to the bands above (below) them needs to be weak so as not to adversely affect transparency.

Following the formulated design principles, we inspect a few hundreds ternary oxides in ICSD [18], looking for near-octet residual valence $|\delta| = 1$ (such as $Ag_3Al_{22}O_{34}$ having $\delta = 1$) with low carrier density. We readily identify two candidate ITC-3 materials: $Ag_3Al_{22}O_{34}$ and $Ba_3Nb_5O_{15}$. Their thermodynamic stability is demonstrated in Supplementary Section I. $Ba_3Nb_5O_{15}$ is found to be stable ground state compounds, whereas $Ag_3Al_{22}O_{34}$ is slightly higher in energy (0.033 eV/atom) than its competing phases ($AgAlO_2$, Ag, and Al_2O_3). However, $Ag_3Al_{22}O_{34}$ is found to satisfy the conditions for ITC-3 better than $Ba_3Nb_5O_{15}$ (see the results of $Ba_3Nb_5O_{15}$ in Supplementary Fig. S6 analogous to the results of $Ag_3Al_{22}O_{34}$ in Fig. 4) due to the sparsity of energy bands near E_F in $Ag_3Al_{22}O_{34}$ (see Fig. 4(a)). The bulk optical absorption coefficient of $Ag_3Al_{22}O_{34}$ (Fig. 4(b)) shows nearly zero absorption for most visible light, except the absorption peak near 3 eV for *z*-polarized light (see green curve in Fig. 4(b)) originating from the interband optical transitions from the partially filled band below E_F to the bands above E_F. The interplay between medium electron density (1.58×10^{21} cm^{-3}) and medium band dispersion (see Fig. 4(a)) leads to small plasma frequencies ($\omega_p^{xx} = \omega_p^{yy} = 1.14$ eV). The calculated transmission spectrum of 1 μm thick slab (Figs. 4(c) and 4(d)) shows an overall transparency of ~70%.

Natural 2-dimensional electron gas (2DEG) forming in a 3D bulk compound: Interestingly, we find that $Ag_3Al_{22}O_{34}$ in the hexagonal $P6_3/mmc$ crystal structure has very high in-plane (*xy*-plane) conductivity ($\sigma^{xx} = \frac{(\omega_p^{xx})^2}{4\pi\gamma} = 0.88\times10^3$ S/cm) but zero out-

of-plane conductivity, *forming a 2DEG in a bulk compound* without the need for Molecular Beam Epitaxy (MBE) synthesized heterostructures with designed modulation doping [27, 28]. Another possible system [29] Ca_2N, does not have a truly 2D electron layer as according to DFT it has rather high out-of-plane conductivity (see Supplementary Fig. S7) in comparison to the pure 2D conductivity in $Ag_3Al_{22}O_{34}$ (Fig. 4). To demonstrate the distribution of carriers in intrinsic TC $Ag_3Al_{22}O_{34}$, we summed the charge density set up by wavefunctions in the energy region indicated by the yellow shading in Fig. 4(a) (between E_F-1 to E_F eV) and obtain the real space electron density shown in Fig. 5(a). We see that the two dimensional electron gas is confined primarily to the Ag-O layers and separated by the Al-O barriers (Fig. 5(a)). The carrier density (Fig. 5(b)) of the 2DEG in the lower Ag-O region is about two times larger than that in the upper Ag-O layer, proportional to the number of Ag atoms (see inset of Fig. 4(b)). As can be seen from the line plot in Fig. 5(b), the width at the half maximum of the 2DEG is 0.2~0.3 nm. Using this 2DEG thickness *the carrier density in the lower Ag-O layer is as high as ~10^{16} cm^{-2}—much higher density than the carrier density achieved in 2DEGs produced in MBE heterostructures* (10^{11}~10^{12} cm^{-2} in semiconductor heterostructures and 10^{13}~10^{14} cm^{-2} in oxide interfaces [28]). The carrier distribution in the intrinsic TCs could be significantly inhomogeneous as in the 2DEGs in Fig. 5. This will contribute to the dependence of ω_p on the plasma wave vector q. In this study, we calculated ω_p (described in Supplementary Section III) for $q = 0$. This is appropriate when considering optical properties for visible light where the photon wave vector $2\pi/\lambda$ (with wavelength λ of 390~700 nm) is considerably smaller than the zone-edge wave vector π/l of the unit cell with l being the lattice constant that is in the order of nm. We note that the spacing (~1 nm) and periodicity (~2 nm) of the alternating higher versus lower density 2DEGs are rather small, thus the 2DEGs can couple with each other. This type of periodic high carrier-density 2DEGs in 3D compounds offers the route to study the mesoscopic collective effects of interacting periodic 2DEGs. The 2D conductivity of 2DEGs is also preferred for the high-performance 2D TC layers in devices for avoiding carrier scattering at the surfaces of TC layers.

Conclusions: The strategy of designing TC's without deliberate doping (Fig. 1(b)) is a particular case of a broader approach of inverse design [11, 30]—starting from physics

based ‘design principles’ (DP), then constructing the ‘design metrics’ (DM) that are computable quantities that embody the physics of the DP, followed by extensive search of materials that score highly on the DM scale, leading to the identification of specific, few ‘best of class’ materials. Here, we extend the initial step of inverse design by revisiting the basic design principles of a selected functionality, leading us to the potentially overlooked prototypes of functional materials, such as the bulk compounds that support free carriers without extrinsic doping while maintaining transparency predicted in this study. Avoidance of deliberate doping (compare Fig. 1(a) with 1(b)) may circumvent structural defects and could thus simplify the manufacturing techniques compared to processes that rely on heavy, and often non-equilibrium doping. Indeed, more extended search of these functionalities, in parallel with stability and growability calculations (exemplified by Figs. S7-S9 in Supplemental Material that includes Refs. [31-34]) along with experimental scrutiny of such results might well be the way to accelerated discovery of functional materials.

Acknowledgements

This work was supported by the U.S. Department of Energy, Office of Science, Basic Energy Sciences. We thank Liping Yu and Giancarlo Trimarchi for helpful discussions.

References

[1] D.S. Ginley, H. Hosono, D.C. Paine, Handbook of Transparent Conductors, Springer Science & Business Media, 2010.

[2] A.V. Moholkar, Transparent Conductors, LAP Lambert Academic Publishing, 2011.

[3] K. Wasa, S. Hayakawa, T. Hada, Electrical and Optical Properties of Sputtered n-p ZnO–Si Heterojunctions, Jpn. J. Appl. Phys. **10**, 1732 (1971).

[4] I. Hamberg, A. Hjortsberg, C.G. Granqvist, High quality transparent heat reflectors of reactively evaporated indium tin oxide, Appl. Phys. Lett. **40**, 362 (1982).

[5] H. Kawazoe, M. Yasukawa, H. Hyodo, M. Kurita, H. Yanagi, H. Hosono, P-type electrical conduction in transparent thin films of CuAlO2, Nature **389**, 939 (1997).

[6] K. Hayashi, S. Matsuishi, T. Kamiya, M. Hirano, H. Hosono, Light-induced conversion of an insulating refractory oxide into a persistent electronic conductor, Nature **419**, 462 (2002).

[7] G.V. Naik, J. Kim, A. Boltasseva, Oxides and nitrides as alternative plasmonic materials in the optical range, Optical Materials Express **1**, 1090 (2011).

[8] H. Mizoguchi, T. Kamiya, S. Matsuishi, H. Hosono, A germanate transparent conductive oxide, Nature Communications **2**, 470 (2011).

[9] A. Kudo, H. Yanagi, H. Hosono, H. Kawazoe, SrCu2O2: A p-type conductive oxide with wide band gap, Appl. Phys. Lett. **73**, 220 (1998).

[10] Ç. Kılıç, A. Zunger, Origins of Coexistence of Conductivity and Transparency in SnO2, Phys. Rev. Lett. **88**, 095501 (2002).

[11] T.R. Paudel, A. Zakutayev, S. Lany, M. d'Avezac, A. Zunger, Doping Rules and Doping Prototypes in A2BO4 Spinel Oxides, Adv. Funct. Mater. **21**, 4493 (2011).

[12] G. Hautier, A. Miglio, G. Ceder, G.-M. Rignanese, X. Gonze, Identification and design principles of low hole effective mass p-type transparent conducting oxides, Nature Communications **4**, 2292 (2013).

[13] E.D. Palik, Handbook of Optical Constants of Solids, Academic Press, Boston, 1998.

[14] K.S. Kim, Y. Zhao, H. Jang, S.Y. Lee, J.M. Kim, K.S. Kim, J.-H. Ahn, P. Kim, J.-Y. Choi, B.H. Hong, Large-scale pattern growth of graphene films for stretchable transparent electrodes, Nature **457**, 706 (2009).

[15] T. Ohsawa, J. Okubo, T. Suzuki, H. Kumigashira, M. Oshima, T. Hitosugi, An n-Type Transparent Conducting Oxide: Nb12O29, J. Phys. Chem. C **115**, 16625 (2011).

[16] J. van de Groep, P. Spinelli, A. Polman, Transparent Conducting Silver Nanowire Networks, Nano Lett. **12**, 3138 (2012).

[17] X. Meng, D. Liu, X. Dai, H. Pan, X. Wen, L. Zuo, G. Qin, Novel stable hard transparent conductors in TiO2-TiC system: Design materials from scratch, Scientific Reports **4**, 7503 (2014).

[18] ICSD, Inorganic Crystal Structure Database; Fachinformationszentrum Karlsruhe: Karlsruhe, Germany, 2006.

[19] W.A. England, A.J. Jacobson, B.C. Tofield, Structural studies of highly non-stoichiometric polycrystalline sodium and silver beta-aluminas, Solid State Ionics **6**, 21 (1982).

[20] B. Hessen, S.A. Sunshine, T. Siegrist, A.T. Fiory, J.V. Waszczak, Structure and Properties of Reduced Barium Niobium Oxide Single Crystals Obtained from Borate Fluxes, Chem. Mater. **3**, 528 (1991).

[21] J.P. Perdew, K. Burke, M. Ernzerhof, Generalized Gradient Approximation Made Simple, Phys. Rev. Lett. **77**, 3865 (1996).

[22] G. Kresse, D. Joubert, From ultrasoft pseudopotentials to the projector augmented-wave method, Phys. Rev. B **59**, 1758 (1999).

[23] J. Heyd, G.E. Scuseria, M. Ernzerhof, Erratum: "Hybrid functionals based on a screened Coulomb potential", J. Chem. Phys. **124**, 219906 (2006).

[24] P. Drude, Zur Elektronentheorie der Metalle, Annalen der Physik **306**, 566 (1900).

[25] J.Z. Hu, I.L. Spain, Phases of silicon at high pressure, Solid State Comm. **51**, 263 (1984).

[26] S. Matsuishi, Y. Toda, M. Miyakawa, K. Hayashi, T. Kamiya, M. Hirano, I. Tanaka, H. Hosono, High-Density Electron Anions in a Nanoporous Single Crystal: [Ca24Al28O64]4+(4e-), Science **301**, 626 (2003).

[27] R. Dingle, H.L. Störmer, A.C. Gossard, W. Wiegmann, Electron mobilities in modulation□doped semiconductor heterojunction superlattices, Appl. Phys. Lett. **33**, 665 (1978).

[28] J. Mannhart, D.G. Schlom, Oxide Interfaces—An Opportunity for Electronics, Science **327**, 1607 (2010).

[29] K. Lee, S.W. Kim, Y. Toda, S. Matsuishi, H. Hosono, Dicalcium nitride as a two-dimensional electride with an anionic electron layer, Nature **494**, 336 (2013).

[30] A. Franceschetti, A. Zunger, The inverse band-structure problem of finding an atomic configuration with given electronic properties, Nature **402**, 60 (1999).

[31] V. Stevanovic, S. Lany, X. Zhang, A. Zunger, Correcting density functional theory for accurate predictions of compound enthalpies of formation: Fitted elemental-phase reference energies, Phys. Rev. B **85**, 115104 (2012).

[32] R. Gautier, X. Zhang, L. Hu, L. Yu, Y. Lin, T.O.L. Sunde, D. Chon, K.R. Poeppelmeier, A. Zunger, Prediction and accelerated laboratory discovery of previously unknown 18-electron ABX compounds, Nature Chemistry **7**, 308 (2015).

[33] X. Zhang, L. Yu, A. Zakutayev, A. Zunger, Sorting Stable versus Unstable Hypothetical Compounds: The Case of Multi- Functional ABX Half-Heusler Filled Tetrahedral Structures, Adv. Funct. Mater. **22**, 1425 (2012).

[34] S.L. Dudarev, G.A. Botton, S.Y. Savrasov, C.J. Humphreys, A.P. Sutton, Electron-energy-loss spectra and the structural stability of nickel oxide: An LSDA+U study, Phys. Rev. B **57**, 1505 (1998).

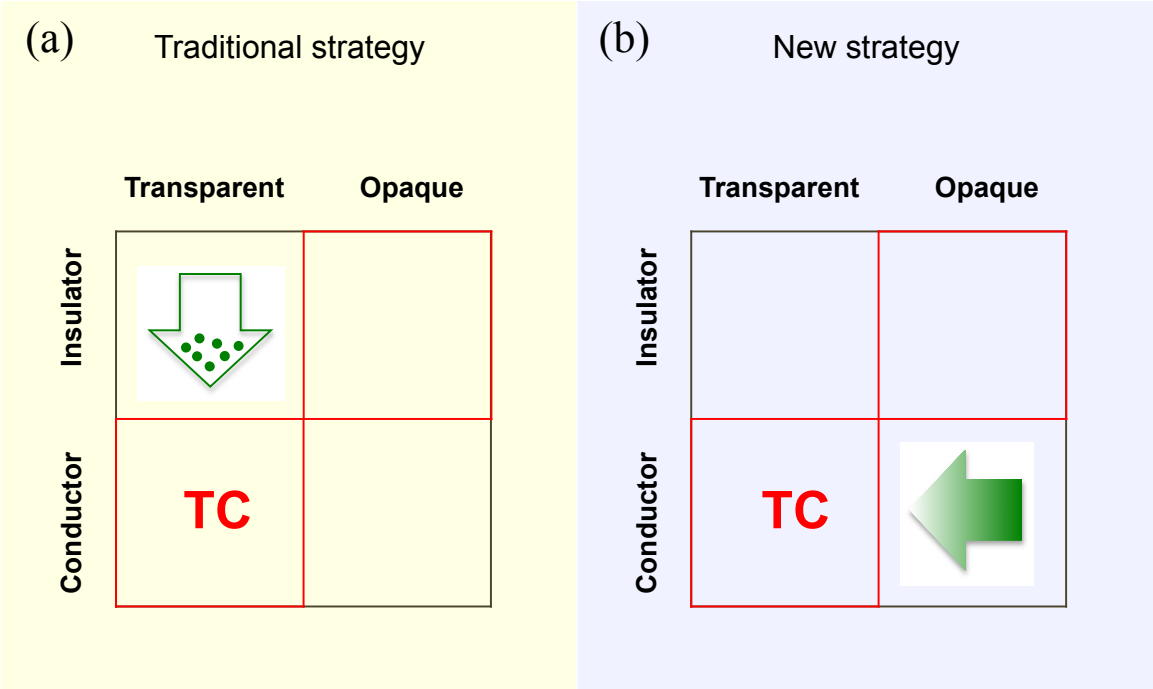

FIG. 1. (a) The traditional strategy for designing bulk transparent conductors that starts from a wide-gap insulator and finds ways to make it conductive by extensive doping without affecting its crystal structure or optical transparency. (b) The new strategy that starts from a metal that already has plenty of free carriers and designs optical transparency to realize an intrinsic (i.e., without intentional chemical doping) TC. This approach requires a technique for controlling the plasma frequency via control of carrier density and band dispersion so the free carrier reflection will not limit transparency.

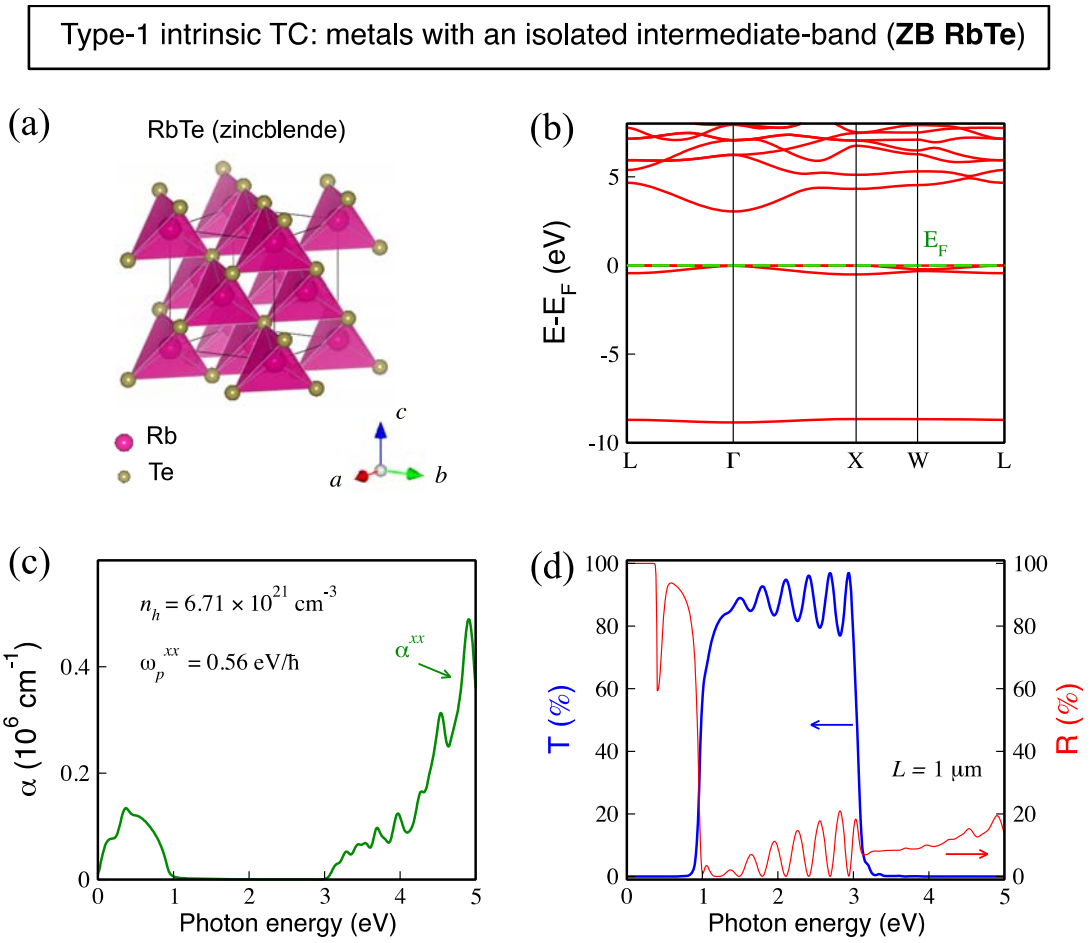

FIG. 2. (a) Crystal structure, (b) band structure and (c) absorption coefficient ($\alpha^{xx} = \alpha^{yy} = \alpha^{zz}$) of zincblende (F-43m) RbTe as an example of type-1 intrinsic TC from DFT. The carrier (hole) concentration (n_h) and plasma frequency ($\omega_p^{xx} = \omega_p^{yy} = \omega_p^{zz}$) are given in (c). The z-axis is chosen along the [001] direction of the cubic lattice. (d) Transmission and reflection spectra of a free standing 1 μm thick RbTe (F-43m) slab with optically smooth surfaces.

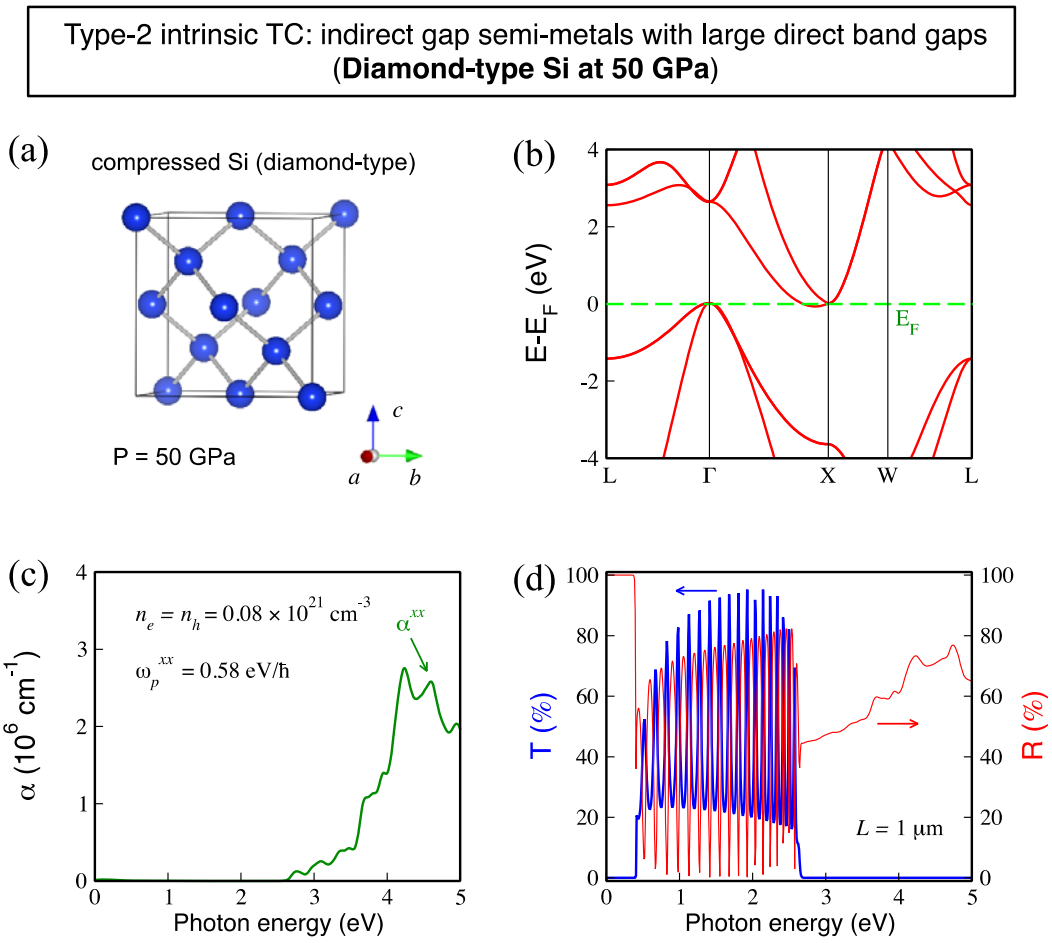

FIG. 3. (a) Crystal structure, (b) band structure and (c) absorption coefficient ($\alpha^{xx} = \alpha^{yy} = \alpha^{zz}$) of compressed diamond-type (Fd-3m) Si under high pressure (P = 50 GPa) as an example of type-2 intrinsic TC from DFT. The carrier (electron and hole) concentration ($n_e = n_h$) and plasma frequency ($\omega_p^{xx} = \omega_p^{yy} = \omega_p^{zz}$) are given in c. The z-axis is chosen along the [001] direction of the cubic lattice. (d) Transmission and reflection spectra of a free standing 1 μm thick compressed Si (Fd-3m) slab with optically smooth surfaces.

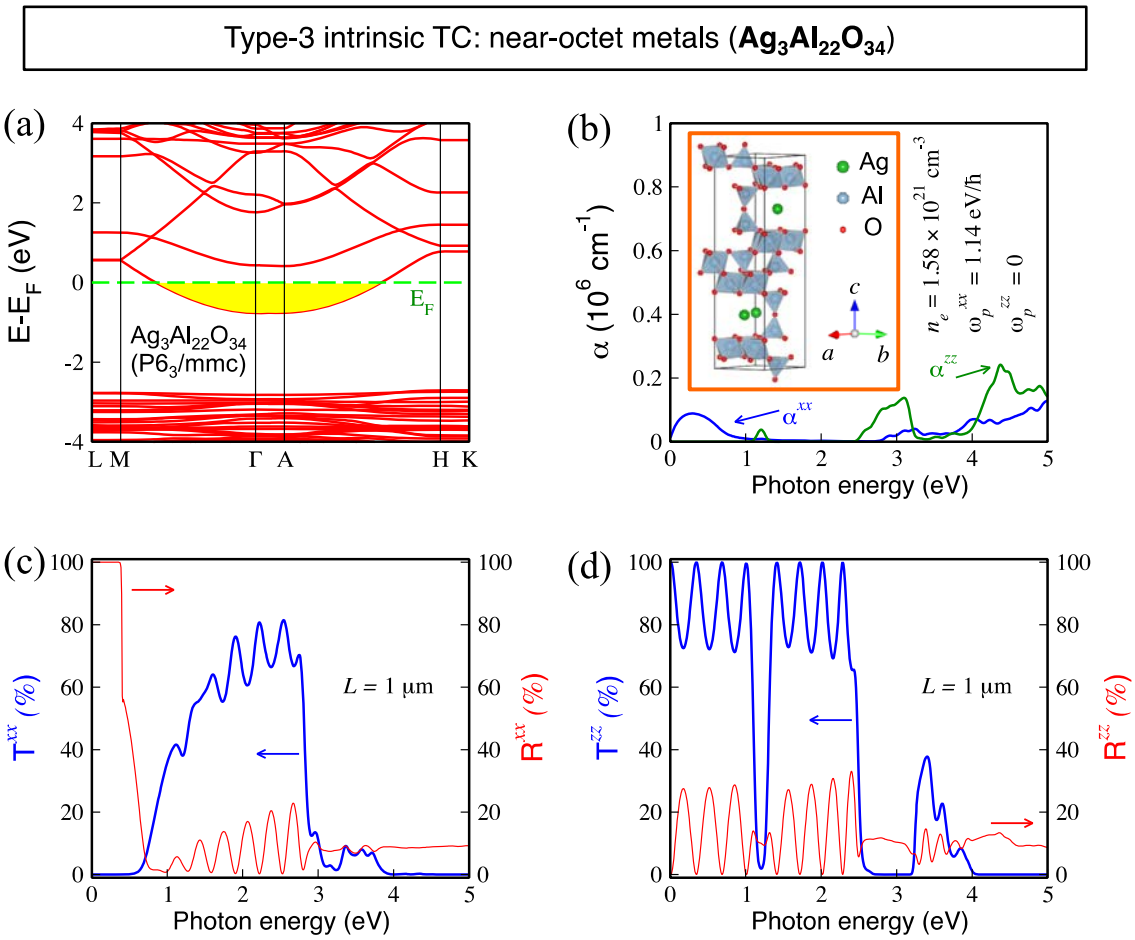

FIG. 4. (a) Band structure, (b) absorption coefficient ($\alpha^{xx} = \alpha^{yy}; \alpha^{zz}$) (inset: crystal structure) of $Ag_3Al_{22}O_{34}$ ($P6_3/mmc$) as an example of type-3 intrinsic TC from DFT. The yellow shading in (a) illustrates the electrons filling the band just below E_F. The carrier (electron) concentration (n_e) and plasma frequency ($\omega_p^{xx} = \omega_p^{yy}; \omega_p^{zz}$) are given in (b). The z-axis is chosen along the [0001] direction of the hexagonal lattice. (c)-(d) Transmission and reflection spectra of a free standing 1 μm thick $Ag_3Al_{22}O_{34}$ slab with optically smooth surfaces.

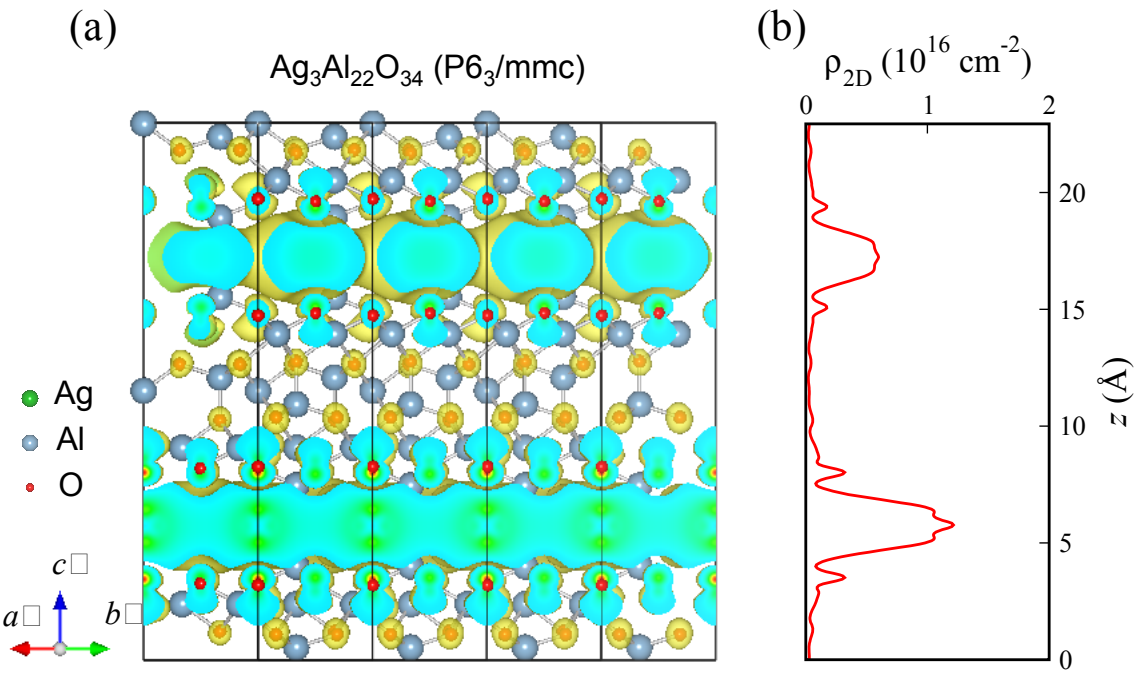

FIG. 5. (a) Real space electron density (isosurface 0.5×10^{21} cm^{-3}) of $Ag_3Al_{22}O_{34}$ ($P6_3/mmc$). (b) Two-dimensional carrier density in *xy*-plane as a function of the position *z*.